═══REVIEW COMMONS MANUSCRIPT═══

IMPORTANT:

- Manuscripts submitted to Review Commons are peer reviewed in a journal-agnostic way.
- Upon transfer of the peer reviewed preprint to a journal, the referee reports will be available in full to the handling editor.
- The identity of the referees will NOT be communicated to the authors unless the reviewers choose to sign their report.
- The identity of the referee will be confidentially disclosed to any affiliate journals to which the manuscript is transferred.

GUIDELINES:

- For reviewers: https://www.reviewcommons.org/reviewers
- For authors: https://www.reviewcommons.org/authors

CONTACT:

The Review Commons office can be contacted directly at: office@reviewcommons.org

# Myotubularin-related proteins regulate KRAS function by controlling plasma membrane levels of polyphosphoinositides and phosphatidylserine

Karen M. Henkels[1], Taylor E. Miller[1], Ali Naji[2], Ransome van der Hoeven[2], Hong Liang[3], Yong Zhou[3], Gerald R.V. Hammond[4] and John F. Hancock[3], Kwang-jin Cho[1, 5]

1. Department of Biochemistry and Molecular Biology, Boonshoft School of Medicine, Wright State University, Dayton, Ohio 45435, USA

2. Department of Diagnostic and Biomedical Sciences, School of Dentistry, The University of Texas Health Science Center at Houston, Houston, Texas 77030, USA

3. Department of Integrative Biology and Pharmacology, McGovern Medical School, University of Texas Health Science Center, Houston, Texas 77030, USA

4. Department of Cell Biology, University of Pittsburgh School of Medicine, Pittsburgh, PA 15213, USA

5. To whom correspondence should be addressed: Kwang-jin Cho, Department of Biochemistry and Molecular Biology, School of Boonshoft Medical School, Wright State University, Dayton, OH 45435; kwang-jin.cho@wright.edu; Tel: (937) 775-2670

**Key words:** Myotubularin-related proteins, phosphatidylserine, KRAS, plasma membrane, phosphatidylinositol, phosphatidylinositol 3-phosphate, phosphatidylinositol 3,5-bisphosphate, phosphatidylinositol 4-phosphate, oxysterol-binding protein related protein (ORP) 5 and 8.

**Abstract** (209 words)

KRAS is a small GTPase, ubiquitously expressed in mammalian cells, that functions as a molecular switch to regulate cell proliferation and differentiation. Oncogenic mutations that render KRAS constitutively active occur frequently in human cancers. KRAS must localize to the plasma membrane (PM) for biological activity. KRAS PM binding is mediated by interactions of the KRAS membrane anchor with phosphatidylserine (PtdSer), therefore, depleting PM PtdSer content abrogates KRAS PM binding and oncogenic function. From a genome-wide siRNA screen to search for genes that regulate KRAS PM localization, we identified a set of phosphatidylinositol (PI) 3-phosphatase family members: myotubularin-related (MTMR) proteins 2, 3, 4 and 7. Here we show that knockdown of *MTMR 2/3/4/7* expression disrupts KRAS PM interactions. The molecular mechanism involves depletion of PM PI 4-phosphate (PI4P) levels, which in turn disrupts the subcellular localization and operation of oxysterol-binding protein related protein (ORP) 5, a PtdSer lipid transfer protein that maintains PM PtdSer content. Concomitantly, silencing *MTMR 2/3/4/7* expression elevates PM levels of PI3P and reduces PM and total cellular levels of PtdSer. In summary we propose that the PI 3-phosphatase activity provided by MTMR proteins is required to generate PM PI for the synthesis of PM PI4P, which in turn, promotes the PM localization of PtdSer and KRAS.

## Introduction

H-, N- and KRAS proteins are small GTPases that oscillate between inactive GDP-bound and active GTP-bound conformational states and operate in signaling cascades that control cell growth and proliferation (Gorfe & Cho, 2019; Henkels *et al*, 2021). Consistent with this key regulatory role, activating mutations of RAS are present in ~20% of human cancers, with the majority occurring in the KRAS isoform (Prior *et al*, 2020). All RAS isoforms must be localized to the inner leaflet of the plasma membrane (PM) and be spatially organized into nanoclusters for biological activity (Gorfe & Cho, 2019; Henkels *et al.*, 2021). Membrane interactions are mediated by the RAS C-terminal membrane anchor (Zhou *et al*, 2017). In the case of KRAS4B, the major expressed splice variant of KRAS (Hood *et al*, 2023) (hereafter KRAS), this anchor comprises a C-terminal farnesyl cysteine methyl ester, generated by posttranslational modification, and an adjacent polybasic domain of six continuous lysines (Gutierrez *et al*, 1989; Hancock *et al*, 1991; Hancock *et al*, 1989; Hancock *et al*, 1990). Recent work has shown that the KRAS membrane anchor encodes exquisite binding specificity for phosphatidylserine (PtdSer) lipids with one saturated and one desaturated acyl chain (Zhou *et al.*, 2017). This lipid binding specificity is effectively hard wired into the anchor structure and renders KRAS PM binding, nanoclustering and hence biological function absolutely dependent on PM PtdSer content (Cho *et al*, 2012b; Cho *et al*, 2013; van der Hoeven *et al*, 2013; van der Hoeven *et al*, 2018).

PtdSer is synthesized in the ER and delivered to the PM against a concentration gradient by the lipid transfer proteins (LTPs), oxysterol-binding protein-related protein (ORP) 5 and 8, operating at ER-PM membrane contact sites. One molecule of phosphatidylinositol (PI) 4-phosphate (P), generated by PM localized PI 4-kinase III$\alpha$ (PI4KA) from PI, is exchanged by ORP5/8 for one molecule of ER localized PtdSer (Chung *et al*, 2015; Moser von Filseck *et al*, 2015). PI4P delivered to the ER is converted to PI by the SAC1 phosphatase, which operating together with PI4KA, maintains the PI4P gradient that in turn, drives PtdSer transport to the PM (Chung *et al.*, 2015; Moser von Filseck *et al.*, 2015). Concordantly genetic and pharmacological studies have shown that inhibition or loss of any component of the PtdSer transport machinery, including PI4KA, EFR3A (the PM anchor protein for the kinase), ORP5, ORP8 and SAC1 results in a reduction in PM PtdSer content, displacement of KRAS from the PM and abrogation of KRAS signaling (Gulyas *et al*, 2017; Kattan *et al*, 2019; Kattan *et al*, 2021; Sohn *et al*, 2018). Other pharmacological approaches to deplete PM PtdSer also dissociate KRAS from the PM (Cho *et al.*, 2012b; Garrido *et al*, 2020; Miller *et al*, 2019; Tan *et al*, 2019; Tan *et al*, 2018; van der Hoeven *et al.*, 2018). The PM is a dynamic organelle, thus KRAS on endomembranes is

sequestered by a chaperone protein, phosphodiesterase 6δ, and released to perinuclear membranes in the ARL2/3-dependent manner. The negative charge on the recycling endosome membranes then electrostatically traps KRAS, from where vesicular transport returns KRAS to the PM (Chandra *et al*, 2012; Schmick *et al*, 2014). KRAS phosphorylation at the Ser181 residue can disrupt this electrostatic interaction, depleting KRAS from the PM (Cho *et al*, 2016a; Kovar *et al*, 2020).

In this context we carried out a cell-based high content screen using a human genomic short interfering (siRNA) library to identify additional potential regulators of KRAS PM localization. Among the hits from the assay were multiple genes that encode proteins with phosphatase activity. Four of these genes encode myotubularin-related (MTMR) proteins 2, 3, 4 and 7, which have 3-phosphatase activity towards phosphatidylinositol (PI) 3-phosphate (P) and PI(3,5)-bisphosphate (PI(3,5)$P_2$) (Robinson & Dixon, 2006). In this study, we examined the role of MTMR proteins in the PM localization of KRAS. Our data demonstrate that knockdown (KD) of MTMR 2, 3, 4 or 7 dissociates KRAS, but not HRAS from the PM. We show *inter alia* that the molecular mechanism involves depletion of the PI4P and PtdSer content of the PM, extending the repertoire of proteins required to support the operation of the ORP5/8 LTPs and hence sustain KRAS PM localization.

## Method and Material

**Plasmids and reagents.** shRNA glycerol sets for MTMR2 (RHS4533-EG8898), MTMR3 (RHS4533-EG8897), MTMR4 (RHS4533-EG9110), MTMR7 (RHS4533-EG9108), and human cDNA of MTMR2 (MHS6278-202760229), MTMR3 (MHS6278-202800229), MTMR4 (MHS6278-202801286) and MTMR7 (MHS6278-211688199) were purchased from GE Healthcare Dharmacon. Antibodies were purchased for detecting MTMR2 (PA5-22748; 1:1,000) from Invitrogen, MTMR3 (sc-393779; 1:1,000) from SCBT and MTMR7 (AB150458; 1:1,000) from Abcam. Anti-ppERK (4370; 1:3,000), anti-pAkt (S473) (4060; 1:1,000), anti-total ERK (4696; 1:1,000), anti-total Akt (2920; 1:1,000) antibodies for immunoblotting were from Cell Signaling Technology. Goat anti-mouse IgG (G21040; 1:2,000), anti-rabbit IgG secondary antibodies (G21234; 1:5,000) and CellMask Deep Red plasma membrane stain (C10046; 1:5,000) were purchased from Invitrogen. Antibodies for detecting β-actin (60008-1-Ig; 1:5,000) and GFP (66002-1-Ig; 1:4,000) were purchased from Proteintech. Staurosporine (BIA-S1086) was purchased from BioAustralis.

**Generating T47D stable cell lines.** T47D cells (ATCC HTB-13) were maintained in RPMI-1640 medium (30-2001, ATCC) supplemented with 10 μg/mL human recombinant insulin (12585-014, Gibco), 2 mM L-glutamine (CA009-010, GenDepot) and 10% FBS (16000044, Life Technologies). Cells were transfected with mGFP-KRASG12V, -HRASG12V or -LactC2 in pEF6 vector (Invitrogen) using *Trans*IT-BrCa Transfection Reagent (MIR 5500, Mirus), and selected with 10 μg/mL blasticidin for 3 weeks. After the selection, cells were maintained in 5 μg/mL blasticidin. For generating MTMR knockdown cell lines, wild-type (WT) T47D cells were infected with lentivirus expressing shRNA targeting *MTMR2, 3, 4* or *7*. Cells were selected by puromycin (1 μg/mL) for 1 week and maintained in 0.5 μg/mL puromycin. Cells were grown at 37$^{o}$C in 5% $CO_2$ and frequently tested for mycoplasma using MycoAlert Mycoplasma Detection Kit (Lonza, LT07-318).

**Preparing T47D cells for imaging.** 5 x $10^5$ T47D cells were seeded on a coverslip on day 1 in RPMI-1640 medium containing 10% FBS, 2mM L-glutamine and 10 μg/mL insulin (complete growth medium). On day 2, fresh complete growth medium was supplemented. On day 3, cells were fixed with 4% PFA for 30 min, quenched with 50 mM $NH_4Cl$ for 10 min and mounted with Vectashield (H-1000, Vector Laboratories). For CellMask staining, cells were incubated with CellMask stain (1:5,000) for 1 h in complete growth medium and fixed with 4% PFA.

**Lipidomic analysis.** T47D cells stably expressing mGFP-KRASG12V with MTMR 2, 3, 4 or 7 knockdown were cultured in complete growth medium containing 0.5 µg/ml puromycin. Triplicate samples of 1x$10^6$ cells were prepared in 333 μL Dulbecco's PBS (DPBS without $Ca^{2+}$ and $Mg^{2+}$, 14190144, Invitrogen). Lipid extraction and analysis using electron spray ionization and MS/ MS were performed at Lipotype GmbH (Dresden, Germany), as described previously (Gerl *et al*, 2012; Sampaio *et al*, 2011). Automated processing of acquired mass spectra, identification, and quantification of detected lipid species were done by LipidXplorer software. Only lipid identifications with a signal-to-noise ratio >5, an absolute abundance of at least 1 pmol, and a signal intensity 5-fold higher than in corresponding blank samples were considered for further data analysis. The abundance of lipids is represented as a heat map with $log_2$ scale relative to control (scrambled shRNA) cells.

**Western blotting.** Preparation of cell lysates and immunoblotting were performed as described previously (Cho *et al*, 2011). Briefly, cells were washed twice with ice-cold 1x phosphate-buffered saline (PBS). Cells were harvested in lysis buffer B containing 50 mM Tris-Cl (pH 7.5),

75 mM NaCl, 25 mM NaF, 5 mM $MgCl_2$, 5 mM EGTA, 1 mM DTT, 100 μM $NaVO_4$, 1% NP-40 plus protease and phosphatase inhibitors. SDS-PAGE and immunoblotting were generally performed using 20–25 μg of lysate from each sample group. Signals were detected by enhanced chemiluminescence (Cat# 34578 and 34075, Thermo Fisher Scientific) and imaged using an Amersham Imager 600 (GE Healthcare). ImageJ software (v1.52) was used to quantify band intensity.

**Validating MTMR4 knockdown.** mRNA was extracted from T47D cells infected with lentivirus expressing shRNA targeting MTMR4 using the RNeasy kit (74104, Qiagen) according to the manufacturer's instructions. 2 μg of total RNA was converted to cDNA using Superscript II reverse transcriptase (18064-014, ThermoFisher). To verify knockdown, forward and reverse primers specific for human MTMR4 exons 1 and 5, and GAPDH (glyceraldehyde-3-phosphate dehydrogenase) exons 1 and 3 were designed: for MTMR4, 5'-CCAAGCCAAGGATCTGTTCCC-3' and 5'-TGTGTGAGACTCTCCAGACGT-'3', and for GAPDH, 5'- GGAGCGAGATCCCTCCAAAAT-3' and 5'-GGCTGTTGTCATACTTCTCATGG-3', respectively. cDNA was amplified by PCR (P2311, GenDepot) and the products were resolved by 1.5% agarose gel electrophoresis and visualized by ethidium bromide staining.

***C. elegans* vulva quantification assay.** *let-60* (n1046) worms were kindly provided by Swathi Arur (MD Anderson Cancer Center, Houston, TX). RNAi was induced by feeding *let-60* worms through adult stage with *E. coli* HT115, producing double-stranded RNA to target genes. The presence of the multivulva phenotype was scored using a DIC/Nomarski microscope. All RNAi clones were from the *C. elegans* RNAi (Ahringer) collection (Source BioScience) and were sequenced.

**Lysenin staining.** A maltose binding protein (MBP)-GFP-lysenin fragment (amino acid residues 161 to 297) was purified as previously described (Maekawa *et al*, 2016). WT T47D cells were fixed with 4% PFA, and permeabilized with 0.05% saponin for 30 min at room temperature (RT), followed by labeling with (15 μg/mL) MBP-GFP-lysenin for 15 min at RT. Cells were quenched with 50 mM $NH_4Cl$ in the dark for 10 min, and further labeled with DAPI (2.5 μg/mL) in the dark for 10 min.

**Proliferation assay.** T47D cells stably expressing mGFP-KRASG12V and MTMR 2, 3, 4 or 7 knockdown were seeded at $1 \times 10^4$ in triplicate onto a 96-well plate in complete growth medium

containing 0.5 μg/mL puromycin. Cells were cultured for 4 days. Fresh complete growth medium containing 0.5 μg/mL puromycin was supplemented every 24 h. On day 5, cell proliferation was assayed by counting cells using Countess II cell counter (Invitrogen).

**Annexin V binding assay.** MTMR 2, 3, 4 or 7 knockdown T47D cells stably expressing mGFP-KRASG12V were incubated with Cy5-conjugated annexin V (559934, BD Pharmingen) according to the manufacturer's instructions. Annexin V-positive cells were counted using a BD AccuriC6 Analyzer with a 670LP nm filter. mGFP-KRASG12V T47D cells expressing scrambled shRNA were treated with 1 μM staurosporine for 6h to induce apoptosis.

**Electron microscopy.** Plasma membrane sheets were prepared from Caco-2 or T47D cells expressing GFP-tagged proteins of interest and fixed as previously described (Hancock & Prior, 2005; Prior *et al*, 2003a; Prior *et al*, 2003b). For univariate analysis, plasma membrane sheets were labeled with anti-GFP antibody conjugated to 4.5-nm gold particles. Digital images of the immunogold-labeled plasma membrane sheets were taken in a transmission electron microscope. Intact 1 $\mu m^2$ areas of the plasma membrane sheet were identified using ImageJ software, and the (x, y) coordinates of the gold particles were determined (Hancock & Prior, 2005; Prior *et al.*, 2003a; Prior *et al.*, 2003b). K-functions (Ripley, 1977) were calculated and standardized on the 99% confidence interval (CI) for univariate functions (Diggle, 2000; Hancock & Prior, 2005; Prior *et al.*, 2003a; Prior *et al.*, 2003b). In the case of univariate functions, a value of L(r)—r greater than the CI indicates significant clustering, and the maximum value of the function ($L_{max}$) estimates the extent of clustering. Differences between replicated point patterns were analyzed by constructing bootstrap tests as described previously (Diggle, 2000; Plowman & Hancock, 2005), and the statistical significance against the results obtained with 1,000 bootstrap samples was evaluated.

## Results

**Genome-wide siRNA screening identifies novel genes regulating KRAS PM interaction.** To identify novel regulators of KRAS PM interaction, we performed an image-based high content screen of a human genomic siRNA library. A Caco-2 (human colorectal adenocarcinoma) cell line stably expressing monomeric green fluorescent protein (GFP)-tagged oncogenic mutant KRAS (KRASG12V) was generated and transfected with siRNA pools comprising four different oligonucleotides against each gene. Four days after transfection, cells

were imaged using an automated confocal microscope to analyze the extent of KRAS mislocalization from the PM. We then narrowed the list of hits using a counter screen against HRASG12V to identify KRASG12V-specific mediators. Bioinformatics analysis revealed that 8 of these putative KRASG12V-specific mediators encode proteins with phosphatase activity (Table 1), 4 of which are members of the myotubularin-related (MTMR) protein family. There are 14 human myotubularins, which exhibit 3-phosphatase activity towards PI3P and PI(3,5)$P_2$, generating PI and PI5P, respectively (Robinson & Dixon, 2006). MTMR proteins have previously been shown to regulate many cellular processes including endocytosis, membrane trafficking, cell proliferation, autophagy, cytokinesis and cytoskeletal dynamics (Hnia *et al*, 2012). We selected this *MTMR* gene set for further analysis.

**MTMR 2/3/4/7 regulate the PM localization of KRASG12V, but not HRASG12V.** To validate the siRNA screen, we generated short-hairpin RNA (shRNA)-mediated stable KD cell lines. T47D (human mammary gland ductal carcinoma) epithelial cells stably expressing GFP-KRASG12V were infected with lentiviruses expressing shRNA targeting *MTMR2, 3, 4* and *7*, followed by puromycin selection. For each target gene, we tested 4 different shRNAs and selected the two most effective KD for further experiments. Immunoblotting verified that endogenous expression levels of MTMR2, 3 and 7 were reduced by the cognate shRNAs (Fig. 1A and S1). MTMR4 mRNA levels were also reduced by shRNA expression; we evaluated mRNA because the anti-MTMR4 antibodies we tested were not able to detect endogenous MTMR4 (Fig. 1A). To study KRAS cellular localization cells were incubated with CellMask, a dye staining cellular membranes (Hu *et al*, 2013; Maechler *et al*, 2019; Monkemoller *et al*, 2015; Park *et al*, 2019), and imaged by confocal microscopy. To quantify the extent of KRAS distribution to endomembranes, we calculated Manders' coefficient, which measures the fraction of CellMask co-localized with GFP-KRASG12V (Cho *et al.*, 2012b; Manders *et al*, 1993; Rehl *et al*, 2023). Our data show that while GFP-KRASG12V is predominantly localized to the PM in control cells, it is distributed intracellularly in the KD cell lines (Fig. 1B). Manders' coefficients for CellMask are correspondingly higher in the KD cell lines, indicating that KRASG12V is redistributed to endomembranes after silencing *MTMR 2/3/4/7*. To directly quantify the extent of KRAS dissociation from the PM, intact basal PM sheets from T47D stably co-expressing GFP-KRASG12V and shRNA for *MTMR 2/3/4/7* were prepared and labeled with gold-conjugated anti-GFP antibodies and analyzed by electron microscopy (EM). We observed significant reductions in anti-GFP immunogold labeling after the KD, indicating loss of KRASG12V from the inner PM leaflet (Fig. 1C and S2). Spatial mapping of GFP-KRASG12V on the PM in *MTMR*

*2/3/4/7* KD cells revealed significant decreases in $L_{max}$, the peak value of the *L(r)-r* clustering statistic that measures the extent of KRAS nanoclustering, which is essential for high-fidelity RAS signal transduction (Cho & Hancock, 2013; Cho *et al*, 2012a; Tian *et al*, 2007) (Fig. 1D). Confocal microscopy further demonstrates that HRASG12V cellular localization is not disrupted after silencing *MTMR 2/3/4/7* (Fig. S3). Together, our data show that MTMR 2/3/4/7 regulate the PM localization and nanoclustering of KRAS, but not HRAS.

**MTMR 2/3/4/7 regulate the cellular level and distribution of PtdSer.** The PM interaction of KRAS, but not HRAS, is dependent on PM PtdSer content (Cho *et al.*, 2012b; Cho *et al*, 2016b; Garrido *et al.*, 2020; Miller *et al.*, 2019; Tan *et al.*, 2018; van der Hoeven *et al.*, 2018; Zhou *et al.*, 2017). To quantify PM PtdSer content, T47D cells stably co-expressing GFP-LactC2, a well-characterized PtdSer probe (Yeung *et al*, 2008), and shRNA targeting *MTMR 2/3/4/7* were incubated with CellMask and imaged by confocal microscopy. GFP-LactC2 is primarily localized to the PM in control cells but is redistributed in *MTMR 2/3/4/7* KD cells as reflected by higher Manders' coefficient values (Fig. 2A and S4). EM analysis of isolated intact PM sheets prepared from T47D cells expressing GFP-LactC2 and incubated with anti-GFP antibody-conjugated gold shows that gold particle labeling density of the inner basal PM is significantly reduced when cells co-express shRNAs for *MTMR 2/3/4/7,* indicating depletion of inner PM PtdSer (Fig. 2B). The loss of inner leaflet PtdSer was not due to flipping to the outer leaflet since Annexin V binding to the outer PM leaflet, as measured by flow cytometry, did not increase in *MTMR 2/3/4/7* KD cells (Fig. S5). Finally, whole cell lipidomics revealed that *MTMR 2/3/4/7* KD resulted in a significant reduction in total cellular PtdSer content (Figs. 2C and D). Together, these results show that MTMR 2/3/4/7 potently regulates the PM and total levels of PtdSer; consistent with a mechanistic role for MTMR 2/3/4/7 in controlling PtdSer cellular distribution.

**MTMR 2/3/4/7 regulate PI4P content at the PM.** In mammalian cells, inner PM leaflet PI4P and PI(4,5)$P_2$ recruit the LTPs ORP5 and ORP8, to ER-PM membrane contact sites (MCSs) to exchange newly synthesized PtdSer in the ER for PI4P from the PM (Chung *et al.*, 2015; Ghai *et al*, 2017; Moser von Filseck *et al.*, 2015; Sohn *et al.*, 2018). Depleting PM PI4P or PI(4,5)$P_2$, concordantly depletes PtdSer and KRAS from the PM (Gulyas *et al.*, 2017; Kattan *et al.*, 2019). Depletion of PI4P at the Golgi complex also mislocalizes PtdSer and KRAS from the PM via an as yet unknown mechanism (Miller *et al.*, 2019). To examine whether silencing *MTMR 2/3/4/7* perturbs cellular localization of PI4P and PI(4,5)$P_2$, *MTMR 2/3/4/7* KD T47D cells expressing GFP-P4M-SidM or GFP-PH-PLC$\delta$1, probes for PI4P (Hammond *et al*, 2014) and PI(4,5)$P_2$

(Varnai & Balla, 1998), respectively, were imaged by confocal microscopy. GFP-P4M-SidM decorated the PM and Golgi complex in control cells (closed and open arrowheads, respectively in Fig. 3A), consistent with previous studies (Hammond *et al.*, 2014; Miller *et al.*, 2019), whereas *MTMR 2/3/4/7* KD perturbed GFP-P4M-SidM staining of the PM, but not the Golgi complex (Fig. 3A). By contrast, the PM localization of GFP-PH-PLCδ1 was unchanged in *MTMR 2/3/4/7* KD cells (Fig. 3A). EM analysis of immunogold labelled PM sheets also shows significant reduction in PI4P PM content, but no change in PI(4,5)$P_2$ PM content after *MTMR 2/3/4/7* KD (Fig. 3B). Given the reduction in PM PI4P content, we next examined ORP5 cellular localization. Confocal imaging showed that GFP-ORP5 predominantly localized to the ER-PM MCS in control cells, but substantially redistributed, presumably, to the ER, in *MTMR 2/3/4/7* KD cells (Fig. 3A) (Du *et al*, 2020; Monteiro-Cardoso *et al*, 2022). We conclude that MTMR 2/3/4/7 regulate ORP5 localization to the ER-PM MCS by maintaining the PM level of PI4P.

***MTMR 2/3/4/7* KD elevates PM PI3P content.** PI3P is synthesized from PI by class II and III PI3Ks, whence it can be converted to PI(3,5)$P_2$ or PI by PI 5-kinase, or myotubularin (MTM) family phosphatases, respectively (Jean & Kiger, 2014; Pulido *et al*, 2013). To examine if depleting MTMR 2/3/4/7 alters cellular PI3P levels or distribution, *MTMR 2/3/4/7* KD T47D cells expressing the well-characterized PI3P probe, GFP-2xFYVE, the tandem FYVE domain of Hrs (hepatocyte growth factor-regulated tyrosine kinase substrate) (Gillooly *et al*, 2000) were stained with CellMask and imaged by confocal microscopy. Mander's coefficient values estimating fractions of endomembranes co-localized with GFP-2xFYVE-decorated endosomes are elevated in *MTMR 3/4/7*, but not *MTMR2*, KD cells, suggesting increased PI3P content in early endosomes (Fig. 4A and B). Moreover, our data show some PM decoration with GFP-2xFYVE in all cells, indicative of PI3P at the PM (arrowheads in Fig. 4A). To formally quantify PM PI3P content, we performed EM analysis on intact basal PM sheets prepared from *MTMR 2/3/4/7* KD T47D cells expressing GFP-2xFYVE. The data reveal that silencing *MTMR 2/3/4/7* significantly elevates PI3P levels in the PM (Fig. 4C). Intriguingly, confocal and EM imaging further show GFP-MTMR 2/3/4/7 localization to the PM (Fig. 4D and E). Together, our data suggest that MTMR 2/3/4/7 localize to the PM, such that genetic depletion disrupts PI3P conversion to PI at the PM, which increases PI3P content at the PM and early endosomes.

**MTMR 2/3/4/7 regulate KRAS signaling.** Since *MTMR 2/3/4/7* KD mislocalizes KRASG12V from the PM, we used two biological systems to evaluate effects on KRAS signal transmission. First, we examined KRAS-transformed T47D cells. Proliferation of *MTMR 2/3/4/7* KD cells stably

expressing GFP-KRASG12V was significantly inhibited compared to parental cells replete for each *MTMR* gene (Fig. 5A). Secondly, we analyzed signaling by the KRAS ortholog, let-60 in the invertebrate model system *Caenorhabditis elegans* (*C. elegans*), where constitutively active mutation of *let-60* induces a quantifiable multivulva phenotype (Reiner *et al*, 2008). We used RNAi designed to target *C. elegans* MTMR orthologs and examined whether *MTMR* KD could suppress the multivulva phenotype associated with expression of LET-60 G13D (n1046). Our data show that silencing *mtm-3* (ortholog of *MTMR3*), or *mtm-6* (ortholog of *MTMR7*) abrogated multivulva formation, and indeed were equipotent with two previously reported potent suppressors of LET-60 G13D signaling (*heo-1* and *riok-1*) (Smith & Levitan, 2004; Weinberg *et al*, 2014) (Fig. 5B). Together, these data provide strong evidence that the MTMR phosphatases regulate KRAS signal transmission by maintaining PtdSer and KRAS PM localization.

## Discussion

We have identified new roles for the phosphatases, MTMR 2/3/4/7, in maintaining the PM localization of PI4P, PtdSer and KRAS. We show that KD of *MTMR 2/3/4/7* dissociates PtdSer and KRAS from the PM and also reduces total cellular PtdSer level. Concomitantly, *MTMR 2/3/4/7* KD elevates PM PI3P content, reduces PM PI4P content and dissociates ORP5 from the ER-PM MCS. Collecting these observations together, we propose that the PM-localized MTMR phosphatases are required to help maintain PM levels of PI for generating PM PI4P by PI4KA, which in turn maintains total PtdSer levels and drives ER to PM transport of PtdSer. PI is synthesized from phosphatidic acid at the cytosolic face of ER, where a fraction of PI is used for the synthesis of glycosylphosphatidylinositol-anchored proteins (Blunsom & Cockcroft, 2020), with the remaining PI being widely distributed across intracellular cytosolic membranes (Ashlin *et al*, 2021; Pemberton *et al*, 2020; Zewe *et al*, 2020). PI delivered from the ER directly to the PM by the LTPs, Nir2/3 and TMEM24 (Posor *et al*, 2022), is a crucial substrate for PM polyphosphoinositides (PPIn). Simple overexpression of Nir2/3 and TMEM24 elevates the synthesis and total amount of PM PPIn (Chang *et al*, 2013; Kim *et al*, 2015; Lees *et al*, 2017), suggesting that PM PI is constantly converted to PPIn and the PI supply to the PM is rate-limiting. In this context, the pathway to PI generation from PI3P by MTMR 2/3/4/7 at the PM, emerges as a critical alternative supplier of PI to allow sufficient PM PI4P generation hence PtdSer transport by the ORP5/8 machinery (Fig. 5C). In addition to the PM, MTMR 2/3/4/7 localize to endosomes and promotes their trafficking by regulating endosomal PI3P and PI(3,5)$P_2$ levels (Bonneick *et al*, 2005; Franklin *et al.*, 2011; Mochizuki & Majerus, 2003; Naughtin *et al.*, 2010; Previtali *et al*, 2007; Walker *et al.*, 2001). Thus, perturbing endosomal

trafficking by *MTMR 2/3/4/7* KD will block the delivery of endosomal PI to the PM, further contributing to the reduced PM PI content. Therefore, when *MTMR 2/3/4/7* is depleted, PM PtdSer level falls and KRAS dissociates from the PM (Fig. 5C). We did not investigate the mechanism whereby *MTMR 2/3/4/7* KD reduced total cellular PtdSer content, but previous work has shown that PM PI4P depletion indirectly blocks PtdSer synthase 1 and 2 activities (Sohn *et al*, 2016). Since PM PI4P levels were reduced in *MTMR 2/3/4/7* KD cells, the same mechanism is likely responsible.

Inactivating mutations in *MTMR2* are found in Charcot-Marie-Tooth disease type 4B1, a severe autosomal recessive neuropathy with demyelination and myelin outfoldings of the nerve. Studies have proposed that disrupted endosomal trafficking by elevating endosomal PI3P and PI(3,5)$P_2$ due to inactive MTMR2 likely contributes to the demyelination of nerve cells (Bonneick *et al.*, 2005; Previtali *et al.*, 2007). Intriguingly, PtdSer is the main component of myelin sheath (Ma *et al*, 2022), and inhibition of PI4KA in Schwann cells reduces PM and total levels of PtdSer and PI4P, and induces aberrant myelination (Alvarez-Prats *et al*, 2018). Thus, in addition to disrupted endosomal trafficking by *MTMR2* inactivation, it is plausible that the reduced PM levels of PtdSer and PI4P further contributes to the demyelination observed in Charcot-Marie-Tooth disease type 4B1.

In sum, our study proposes a new role for the MTMR phosphatases in maintaining PM PI4P and PtdSer contents by maintaining an adequate supply of PM PI from PI3P. Depleting MTMR 2/3/4/7 in turn, reduces PM and total cellular PtdSer levels, blocking KRAS PM localization and KRAS signaling. Thus, the mechanisms that maintain PM PI content may be contain useful targets to abrogate oncogenic KRAS signaling.

**Acknowledgements**

This work was supported by Wright State University Seed Grant and the National Cancer Institute [R00-CA188593 to K.-J.C.], National Institutes of Health [2R35GM119412 to G.R.V. Hammond] and The Cancer Prevention and Research Institute of Texas [CPRIT RP200047 to JFH].

**Figure legend**

**Table 1. 8 novel genes, which encode proteins with phosphatase activity are identified to regulate KRAS/PM localization.**

PI – phosphatidylinositol, Ins – inositol, MTMR – myotubularin-related protein, MINPP1 – multiple inositol-polyphosphate phosphatase 1, TMEM55A – transmembrane protein 55A, INPPL1 - inositol polyphosphate phosphatase Like 1, SHIP2 – SH2-containing phosphatidylinositol 3,4,5-trisphosphate 5-phosphatase, PPP2R5B - protein phosphatase 2 regulatory subunit β

**Figure 1. MTMR 2/3/4/7 regulate the PM localization of KRASG12V.** (**A**) T47D cells stably expressing GFP-KRASG12V were infected with lentivirus expressing scrambled shRNA (SCR) or shRNA targeting *MTMR2, 3, 4* or *7*, followed by 1 ug/mL puromycin selection. Cell lysates were prepared and immunoblotted with anti-MTMR2, 3 or 7 antibodies. Actin blots are shown as loading controls. For MTMR4, cDNA was amplified with primers specific for MTMR4 exons 1 and 5, or GAPDH exons 2 and 3 as a loading control. (**B**) These cells were incubated with CellMask for 1 h at 37$^{o}$C incubator, fixed with 4% PFA and imaged by confocal microscopy. Representative GFP-KRASG12V images are shown. Their corresponding CellMask and merged images are shown in Fig. S2. The inserted values represent a mean fraction ± S.E.M. of CellMask colocalizing with GFP-KRASG12V calculated by Manders' coefficient from three independent experiments. Scale bar – 10 μm. (**C**) Intact basal PM sheets prepared from T47D cells co-expressing GFP-KRASG12V and shRNA targeting *MTMR2, 3, 4* or *7* were labeled with anti-GFP-conjugated gold particles and visualized by EM. Representative EM images are shown in Fig. S3. The graphs show a mean number of gold particles ± SEM (n ≥ 15). (**D**) Spatial mapping of the same gold-labeled PM sheets was performed. The peak values, $L_{max}$, representing the extent of KRAS spatial organization, are shown as bar graphs (n ≥ 15). Significant differences between control (SCR-expressing) and *MTMR*-silenced cells were assessed by one-way ANOVA test for (B and C) and bootstrap tests for (D) (* $p < 0.05$, ** $p < 0.01$, *** $p < 0.001$, **** $p < 0.0001$).

**Figure 2. MTMR 2/3/4/7 regulate the cellular level and distribution of PtdSer.** (**A**) T47D cells stably expressing GFP-LactC2 were infected with lentivirus expressing scrambled shRNA (SCR) or shRNA targeting *MTMR2, 3, 4* or *7*, followed by 1 ug/mL puromycin selection. Cells were incubated with CellMask for 1 h at 37$^{o}$C incubator, fixed with 4% PFA and imaged by confocal microscopy. Representative GFP-LactC2 images are shown. Their corresponding CellMask and

merged images are shown in Fig. S5. The inserted values represent a mean fraction ± S.E.M. of CellMask colocalizing with GFP-LactC2 calculated by Manders' coefficient from three independent experiments. Scale bar – 10 μm. (**B**) Intact basal PM sheets prepared from T47D cells co-expressing GFP-LactC2 and shRNA targeting *MTMR2, 3, 4* or *7* were labeled with anti-GFP-conjugated gold particles and visualized by EM. The graphs show a mean number of gold particles ± SEM (n ≥ 15). (**C**) Whole cell PtdSer levels were measured in these cells via electron spray ionization and MS/MS from three independent experiments. A heat map was constructed to quantify the changes of different lipid species after *MTMR* knockdown. Each row represents a different species of PtdSer, while each column represents a single sample. The scaled expression values of each lipid measured is plotted in red-blue color $\log_2$ scale. In relation to control (SCR) cells, red and blue colored tiles indicate higher and lower lipid contents, respectively. (**D**) The graph shows the mean of total moles ± S.E.M. of PtdSer. Significant differences between control (SCR-expressing) and *MTMR*-silenced cells were assessed using one-way ANOVA tests (* $p < 0.05$, ** $p < 0.01$, *** $p < 0.001$, **** $p < 0.0001$, # – not significant).

**Figure 3. MTMR 2/3/4/7 regulate the localization of PM PI4P and ORP5.** (**A**) WT T47D cells were infected with lentivirus expressing scrambled shRNA (SCR) or shRNA targeting *MTMR2, 3, 4* or *7*, followed by 1 ug/mL puromycin selection. These cells were transfected with GFP-P4M-SidM, -PH-PLCδ1, or -ORP5, and fixed with 4% PFA and imaged by confocal microscopy. Closed and open arrowheads for GFP-P4M-SidM indicate the staining of PM and Golgi complex, respectively. Closed arrowheads for GFP-ORP5 indicate the ER localization of ORP5. Scale bar – 10 μm. Intact basal PM sheet of Caco-2 cells co-expressing GFP-P4M-SidM (**B**) or -PH-PLCδ1 (**C**) with shRNA targeting *MTMR2, 3, 4,* or *7* were labeled with anti-GFP-conjugated gold particles and visualized by EM. The graphs show a mean number of gold particles ± SEM (n ≥ 15). Significant differences between control (SCR-expressing) and *MTMR*-silenced cells were assessed by one-way ANOVA tests (* $p < 0.05$, **** $p < 0.0001$, # – not significant).

**Figure 4. MTMR 2/3/4/7 regulate cellular PI3P contents.** (**A**) T47D cells expressing scrambled shRNA (SCR) or shRNA targeting *MTMR2, 3, 4* or *7*, followed by 1 ug/mL puromycin selection, were overexpressed with GFP-2xFYVE. Cells were incubated with CellMask for 1 h at 37$^{o}$C incubator, fixed with 4% PFA and imaged by confocal microscopy. Representative GFP-2xFYVE images are shown. Their corresponding CellMask and merged images are shown in Fig. S7. A selected region (the white square) is shown at a higher magnification. Arrowheads indicate the PM-staining of GFP-2xFYVE. (**B**) The graph represents a mean fraction ± S.E.M (n

= 13) of CellMask colocalizing with GFP-2xFYVE calculated by Manders' coefficient (**C**) Intact basal PM sheets prepared from these T47D cells from (A), or WT T47D cells expressing GFP-MTMR proteins (**D**) were labeled with anti-GFP-conjugated gold particles and visualized by EM. The graphs show a mean number of gold particles ± SEM (n ≥ 15). (**E**) Cells from (D) were fixed with 4% PFA and imaged by confocal microscopy. Scale bar – 10 μm. Arrowheads indicate the PM localization of MTMR proteins. Significant differences between control (SCR-expressing) and *MTMR*-silenced cells were assessed by one-way ANOVA test for (B and C) (* $p < 0.05$, ** $p < 0.01$, *** $p < 0.001$, **** $p < 0.0001$, # - not significant). Significant differences between untagged GFP (control) and GFP-MTMR-expressing cells were assessed by one-way ANOVA test for (D) (** $p < 0.01$, *** $p < 0.001$, **** $p < 0.0001$).

**Figure 5. MTMR 2/3/4/7 regulate cell growth and *C. elegans* transformed by oncogenic KRAS.** (**A**) T47D cells stably expressing GFP-KRASG12V were infected with lentivirus expressing scrambled shRNA (SCR) or shRNA targeting *MTMR2, 3, 4* or *7*, followed by 1 ug/mL puromycin selection. Cells were seeded on a 96-well plate and cultured for 4 days. Complete growth medium was replaced every 24 h. Cell numbers were counted to measure cell proliferation. The graph shows the mean cell proliferation ± S.E.M. from three independent experiments relative to that for the control cells (SCR-expressing). Significant differences between control and *MTMR* knockdown cells were assessed using one-way ANOVA test (* $p<0.05$, ** $p<0.01$, *** $p<0.001$). (**B**) RNAi was induced by feeding *let-60* (n1046) L1 worms through adult stage with *E. coli* strain HT115, producing dsRNA to target genes. The presence of the multi-vulva phenotype was scored using DIC/Nomarski microscopy. 100 – 200 worms were assayed per RNAi knockdown. Significant differences were evaluated in Student's *t*-tests (** $p < 0.01$ and *** $p < 0.001$).

**Figure 6. A working model of our study.** PITPs deliver newly synthesized PI from the ER to PM, and MTMR at the PM concomitantly converts PI3P to PI, which are which are crucial substrate for PM PPIn like PI4P. ORP5 and 8, the lipid transfer proteins for PtdSer, exchanges ER PtdSer with PM PI4P at ER-PM membrane-contacting sites, which enriches PM PtdSer contents. This, in turn, allows stable PM binding of KRAS, and thereby KRAS signal output. When MTMR is depleted, PM PI3P conversion to PI is blocked, providing insufficient PM PI contents for PI4P synthesis. This dissociates ORP5/8 from ER-PM membrane-contacting sites, resulting in reduced PM localization of PtdSer and thereby KRAS. PITPs – PI transfer proteins,

PI4KA – phosphatidylinositol 4-kinase III$\alpha$, ORP – oxysterol-binding protein related protein, PM – plasma membrane, ER – endoplasmic reticulum.

**Supplement Figure 1. Identifying shRNAs for silencing *MTMR 2, 3* or *7*.** T47D cells were infected with lentivirus expressing scrambled shRNA (SCR) or shRNA targeting *MTMR2, 3, 4* or *7*, followed by 1 ug/mL puromycin selection. Cell lysates were immunoblotted for MTMR2, 3, or 7. GAPDH blots are shown as loading controls. mRNA from for T4D cells expressing shRNA targeting *MTMR4* was extracted and converted to cDNA, followed by amplification by PCR. The amplicons were resolved by 1.5% agarose gel electrophoresis. Cell lysates and mRNA of HEK293T cells expressing human cDNA of MTMR 2, 3 or 7, and MTMR4, respectively, were used as a positive control. Arrowheads indicate the protein of interest.

**Supplement Figure 2. MTMR 2/3/4/7 regulate the PM localization of KRASG12V.** T47D cells stably expressing GFP-KRASG12V were infected with lentivirus expressing scrambled shRNA (SCR) or shRNA targeting *MTMR2, 3, 4* or *7*, followed by 1 ug/mL puromycin selection. Cells were incubated with CellMask for 1 h at 37$^{o}$C incubator, fixed with 4% PFA and imaged by confocal microscopy. The inserted values represent a mean fraction $\pm$ S.E.M. of CellMask colocalizing with GFP-KRASG12V calculated by Manders' coefficient from three independent experiments. Scale bar – 10 $\mu$m. Significant differences between control (SCR-expressing) and *MTMR*-silenced cells were assessed by one-way ANOVA test for (C) and bootstrap tests for (D) (* $p < 0.05$, ** $p < 0.01$, *** $p < 0.001$, **** $p < 0.0001$).

**Supplement Figure 3. MTMR 2/3/4/7 regulate the PM localization of KRAS.** Intact basal PM sheets prepared from T47D cells co-expressing GFP-KRASG12V and shRNA targeting *MTMR2, 3, 4* or *7* were labeled with anti-GFP-conjugated gold particles and visualized by EM. Representative EM images are shown. Scale bar – 0.1 $\mu$m.

**Supplement Figure 4. *MTMR 2/3/4/7* KD does not alter HRAS/PM localization.** (**A**) T47D cells stably expressing GFP-HRASG12V were infected with lentivirus expressing scrambled shRNA (SCR) or shRNA targeting *MTMR2, 3, 4* or *7*, followed by 1 ug/mL puromycin selection. These cells were incubated with CellMask Deep Red for 1 h at 37$^{o}$C incubator, fixed with 4% PFA and imaged by confocal microscopy. (B) The graphs represent a mean fraction $\pm$ S.E.M. of CellMask colocalizing with GFP-HRASG12V calculated by Manders' coefficient from three independent experiments. Significant differences between control (scrambled shRNA, SCR) and

*MTMR* knockdown cells were assessed using a one-way ANOVA test (N.S. – not significant). Scale bar – 10 μm.

**Supplement Figure 5. MTMR 2/3/4/7 regulates PtdSer cellular distribution.** (**A**) T47D cells stably expressing GFP-LactC2 were infected with lentivirus expressing scrambled shRNA (SCR) or shRNA targeting *MTMR2, 3, 4* or *7*, followed by 1 ug/mL puromycin selection. Cells were incubated with CellMask for 1 h at 37$^{o}$C incubator, fixed with 4% PFA and imaged by confocal microscopy. The inserted values represent a mean fraction ± S.E.M. of CellMask colocalizing with GFP-LactC2 calculated by Manders' coefficient from three independent experiments. Scale bar – 10 μm.

**Supplement Figure 6. MTMR 2/3/4/7 do not externalize cellular PtdSer.** T47D stably expressing GFP-KRASG12V were infected with lentivirus expressing scrambled shRNA (SCR) or shRNA targeting *MTMR2, 3, 4* or *7*, followed by 1 ug/mL puromycin selection. Cells were incubated with Cy5-conjugated annexin V and annexin V-positive cells were counted by flow cytometry. SCR cells were treated with 1 μM staurosporine (STS) for 6 h to induce apoptosis. The graph represents a mean (%) ± S.E.M. of annexin V-positive cells from three independent experiments. Significant differences between control (SCR-expressing) and *MTMR*-silenced cells were assessed by one-way ANOVA test (**** $p < 0.0001$, N.S. – not significant).

**Supplement Figure 7. MTMR 2/3/4/7 regulate cellular PI3P contents.** T47D cells expressing scrambled shRNA (SCR) or shRNA targeting *MTMR2, 3, 4* or *7*, followed by 1 ug/mL puromycin selection, were overexpressed with GFP-2xFYVE. Cells were incubated with CellMask for 1 h at 37$^{o}$C incubator, fixed with 4% PFA and imaged by confocal microscopy. A selected region (the white square) is shown at a higher magnification. Arrowheads indicate the PM-staining of GFP-2xFYVE.

## Reference


Alvarez-Prats A, Bjelobaba I, Aldworth Z, Baba T, Abebe D, Kim YJ, Stojilkovic SS, Stopfer M, Balla T (2018) Schwann-Cell-Specific Deletion of Phosphatidylinositol 4-Kinase Alpha Causes Aberrant Myelination. *Cell Rep* 23: 2881-2890

Ashlin TG, Blunsom NJ, Cockcroft S (2021) Courier service for phosphatidylinositol: PITPs deliver on demand. *Biochim Biophys Acta Mol Cell Biol Lipids* 1866: 158985

Blunsom NJ, Cockcroft S (2020) Phosphatidylinositol synthesis at the endoplasmic reticulum. *Biochim Biophys Acta Mol Cell Biol Lipids* 1865: 158471

Bonneick S, Boentert M, Berger P, Atanasoski S, Mantei N, Wessig C, Toyka KV, Young P, Suter U (2005) An animal model for Charcot-Marie-Tooth disease type 4B1. *Hum Mol Genet* 14: 3685-3695

Chandra A, Grecco HE, Pisupati V, Perera D, Cassidy L, Skoulidis F, Ismail SA, Hedberg C, Hanzal-Bayer M, Venkitaraman AR *et al* (2012) The GDI-like solubilizing factor PDEdelta sustains the spatial organization and signalling of Ras family proteins. *Nat Cell Biol* 14: 148-158

Chang CL, Hsieh TS, Yang TT, Rothberg KG, Azizoglu DB, Volk E, Liao JC, Liou J (2013) Feedback regulation of receptor-induced Ca2+ signaling mediated by E-Syt1 and Nir2 at endoplasmic reticulum-plasma membrane junctions. *Cell Rep* 5: 813-825

Cho KJ, Casteel DE, Prakash P, Tan L, van der Hoeven D, Salim AA, Kim C, Capon RJ, Lacey E, Cunha SR *et al* (2016a) AMPK and Endothelial Nitric Oxide Synthase Signaling Regulates K-Ras Plasma Membrane Interactions via Cyclic GMP-Dependent Protein Kinase 2. *Mol Cell Biol* 36: 3086-3099

Cho KJ, Hancock JF (2013) Ras nanoclusters: a new drug target? *Small GTPases* 4: 57-60

Cho KJ, Hill MM, Chigurupati S, Du G, Parton RG, Hancock JF (2011) Therapeutic levels of the hydroxmethylglutaryl-coenzyme A reductase inhibitor lovastatin activate ras signaling via phospholipase D2. *Mol Cell Biol* 31: 1110-1120

Cho KJ, Kasai RS, Park JH, Chigurupati S, Heidorn SJ, van der Hoeven D, Plowman SJ, Kusumi A, Marais R, Hancock JF (2012a) Raf inhibitors target ras spatiotemporal dynamics. *Curr Biol* 22: 945-955

Cho KJ, Park JH, Piggott AM, Salim AA, Gorfe AA, Parton RG, Capon RJ, Lacey E, Hancock JF (2012b) Staurosporines disrupt phosphatidylserine trafficking and mislocalize Ras proteins. *J Biol Chem* 287: 43573-43584

Cho KJ, van der Hoeven D, Hancock JF (2013) Inhibitors of K-Ras plasma membrane localization. *Enzymes* 33 Pt A: 249-265

Cho KJ, van der Hoeven D, Zhou Y, Maekawa M, Ma X, Chen W, Fairn GD, Hancock JF (2016b) Inhibition of Acid Sphingomyelinase Depletes Cellular Phosphatidylserine and Mislocalizes K-Ras from the Plasma Membrane. *Mol Cell Biol* 36: 363-374

Chung J, Torta F, Masai K, Lucast L, Czapla H, Tanner LB, Narayanaswamy P, Wenk MR, Nakatsu F, De Camilli P (2015) INTRACELLULAR TRANSPORT. PI4P/phosphatidylserine

countertransport at ORP5- and ORP8-mediated ER-plasma membrane contacts. *Science* 349: 428-432

Diggle PJ, J. Mateu, and H. E. Clough. (2000) A comparison between parametric and non-parametric approaches to the analysis of replicated spatial point patterns. *Adv Appl Probab* 32: 331-343

Du X, Zhou L, Aw YC, Mak HY, Xu Y, Rae J, Wang W, Zadoorian A, Hancock SE, Osborne B *et al* (2020) ORP5 localizes to ER-lipid droplet contacts and regulates the level of PI(4)P on lipid droplets. *J Cell Biol* 219

Franklin NE, Taylor GS, Vacratsis PO (2011) Endosomal targeting of the phosphoinositide 3-phosphatase MTMR2 is regulated by an N-terminal phosphorylation site. *J Biol Chem* 286: 15841-15853

Garrido CM, Henkels KM, Rehl KM, Liang H, Zhou Y, Gutterman JU, Cho KJ (2020) Avicin G is a potent sphingomyelinase inhibitor and blocks oncogenic K- and H-Ras signaling. *Sci Rep* 10: 9120

Gerl MJ, Sampaio JL, Urban S, Kalvodova L, Verbavatz JM, Binnington B, Lindemann D, Lingwood CA, Shevchenko A, Schroeder C *et al* (2012) Quantitative analysis of the lipidomes of the influenza virus envelope and MDCK cell apical membrane. *J Cell Biol* 196: 213-221

Ghai R, Du X, Wang H, Dong J, Ferguson C, Brown AJ, Parton RG, Wu JW, Yang H (2017) ORP5 and ORP8 bind phosphatidylinositol-4, 5-biphosphate (PtdIns(4,5)P 2) and regulate its level at the plasma membrane. *Nat Commun* 8: 757

Gillooly DJ, Morrow IC, Lindsay M, Gould R, Bryant NJ, Gaullier JM, Parton RG, Stenmark H (2000) Localization of phosphatidylinositol 3-phosphate in yeast and mammalian cells. *EMBO J* 19: 4577-4588

Gorfe AA, Cho KJ (2019) Approaches to inhibiting oncogenic K-Ras. *Small GTPases*: 1-10

Gulyas G, Radvanszki G, Matuska R, Balla A, Hunyady L, Balla T, Varnai P (2017) Plasma membrane phosphatidylinositol 4-phosphate and 4,5-bisphosphate determine the distribution and function of K-Ras4B but not H-Ras proteins. *J Biol Chem* 292: 18862-18877

Gutierrez L, Magee AI, Marshall CJ, Hancock JF (1989) Post-translational processing of p21ras is two-step and involves carboxyl-methylation and carboxy-terminal proteolysis. *EMBO J* 8: 1093-1098

Hammond GR, Machner MP, Balla T (2014) A novel probe for phosphatidylinositol 4-phosphate reveals multiple pools beyond the Golgi. *J Cell Biol* 205: 113-126

Hancock JF, Cadwallader K, Paterson H, Marshall CJ (1991) A CAAX or a CAAL motif and a second signal are sufficient for plasma membrane targeting of ras proteins. *Embo J* 10: 4033-4039

Hancock JF, Magee AI, Childs JE, Marshall CJ (1989) All ras proteins are polyisoprenylated but only some are palmitoylated. *Cell* 57: 1167-1177

Hancock JF, Paterson H, Marshall CJ (1990) A polybasic domain or palmitoylation is required in addition to the CAAX motif to localize p21ras to the plasma membrane. *Cell* 63: 133-139

Hancock JF, Prior IA (2005) Electron microscopic imaging of Ras signaling domains. *Methods* 37: 165-172

Henkels KM, Rehl KM, Cho KJ (2021) Blocking K-Ras Interaction With the Plasma Membrane Is a Tractable Therapeutic Approach to Inhibit Oncogenic K-Ras Activity. *Front Mol Biosci* 8: 673096

Hnia K, Vaccari I, Bolino A, Laporte J (2012) Myotubularin phosphoinositide phosphatases: cellular functions and disease pathophysiology. *Trends Mol Med* 18: 317-327

Hood FE, Sahraoui YM, Jenkins RE, Prior IA (2023) Ras protein abundance correlates with Ras isoform mutation patterns in cancer. *Oncogene* 42: 1224-1232

Hu Y, Wan JM, Yu AC (2013) Membrane perforation and recovery dynamics in microbubble-mediated sonoporation. *Ultrasound Med Biol* 39: 2393-2405

Jean S, Kiger AA (2014) Classes of phosphoinositide 3-kinases at a glance. *J Cell Sci* 127: 923-928

Kattan WE, Chen W, Ma X, Lan TH, van der Hoeven D, van der Hoeven R, Hancock JF (2019) Targeting plasma membrane phosphatidylserine content to inhibit oncogenic KRAS function. *Life Sci Alliance* 2

Kattan WE, Liu J, Montufar-Solis D, Liang H, Brahmendra Barathi B, van der Hoeven R, Zhou Y, Hancock JF (2021) Components of the phosphatidylserine endoplasmic reticulum to plasma membrane transport mechanism as targets for KRAS inhibition in pancreatic cancer. *Proc Natl Acad Sci U S A* 118

Kim YJ, Guzman-Hernandez ML, Wisniewski E, Balla T (2015) Phosphatidylinositol-Phosphatidic Acid Exchange by Nir2 at ER-PM Contact Sites Maintains Phosphoinositide Signaling Competence. *Dev Cell* 33: 549-561

Kovar SE, Fourman C, Kinstedt C, Williams B, Morris C, Cho KJ, Ketcha DM (2020) Chalcones bearing a 3,4,5-trimethoxyphenyl motif are capable of selectively inhibiting oncogenic K-Ras signaling. *Bioorg Med Chem Lett* 30: 127144

Lees JA, Messa M, Sun EW, Wheeler H, Torta F, Wenk MR, De Camilli P, Reinisch KM (2017) Lipid transport by TMEM24 at ER-plasma membrane contacts regulates pulsatile insulin secretion. *Science* 355

Ma X, Li X, Wang W, Zhang M, Yang B, Miao Z (2022) Phosphatidylserine, inflammation, and central nervous system diseases. *Front Aging Neurosci* 14: 975176

Maechler FA, Allier C, Roux A, Tomba C (2019) Curvature-dependent constraints drive remodeling of epithelia. *J Cell Sci* 132

Maekawa M, Lee M, Wei K, Ridgway ND, Fairn GD (2016) Staurosporines decrease ORMDL proteins and enhance sphingomyelin synthesis resulting in depletion of plasmalemmal phosphatidylserine. *Sci Rep* 6: 35762

Manders EMM, Verbeek FJ, Aten JA (1993) Measurement of co-localization of object in dual-colour confocal images. *Journal of Microscopy* 169: 375-382

Miller TE, Henkels KM, Huddleston M, Salisbury R, Hussain SM, Sasaki AT, Cho KJ (2019) Depletion of phosphatidylinositol 4-phosphate at the Golgi translocates K-Ras to mitochondria. *J Cell Sci* 132

Mochizuki Y, Majerus PW (2003) Characterization of myotubularin-related protein 7 and its binding partner, myotubularin-related protein 9. *Proc Natl Acad Sci U S A* 100: 9768-9773

Monkemoller V, Oie C, Hubner W, Huser T, McCourt P (2015) Multimodal super-resolution optical microscopy visualizes the close connection between membrane and the cytoskeleton in liver sinusoidal endothelial cell fenestrations. *Sci Rep* 5: 16279

Monteiro-Cardoso VF, Rochin L, Arora A, Houcine A, Jaaskelainen E, Kivela AM, Sauvanet C, Le Bars R, Marien E, Dehairs J *et al* (2022) ORP5/8 and MIB/MICOS link ER-mitochondria and intra-mitochondrial contacts for non-vesicular transport of phosphatidylserine. *Cell Rep* 40: 111364

Moser von Filseck J, Copic A, Delfosse V, Vanni S, Jackson CL, Bourguet W, Drin G (2015) INTRACELLULAR TRANSPORT. Phosphatidylserine transport by ORP/Osh proteins is driven by phosphatidylinositol 4-phosphate. *Science* 349: 432-436

Naughtin MJ, Sheffield DA, Rahman P, Hughes WE, Gurung R, Stow JL, Nandurkar HH, Dyson JM, Mitchell CA (2010) The myotubularin phosphatase MTMR4 regulates sorting from early endosomes. *J Cell Sci* 123: 3071-3083

Park S, Joo YK, Chen Y (2019) Versatile and High-throughput Force Measurement Platform for Dorsal Cell Mechanics. *Sci Rep* 9: 13286

Pemberton JG, Kim YJ, Humpolickova J, Eisenreichova A, Sengupta N, Toth DJ, Boura E, Balla T (2020) Defining the subcellular distribution and metabolic channeling of phosphatidylinositol. *J Cell Biol* 219

Plowman SJ, Hancock JF (2005) Ras signaling from plasma membrane and endomembrane microdomains. *Biochim Biophys Acta* 1746: 274-283

Posor Y, Jang W, Haucke V (2022) Phosphoinositides as membrane organizers. *Nat Rev Mol Cell Biol* 23: 797-816

Previtali SC, Quattrini A, Bolino A (2007) Charcot-Marie-Tooth type 4B demyelinating neuropathy: deciphering the role of MTMR phosphatases. *Expert Rev Mol Med* 9: 1-16

Prior IA, Hood FE, Hartley JL (2020) The frequency of Ras mutations in cancer. *Cancer Res*

Prior IA, Muncke C, Parton RG, Hancock JF (2003a) Direct visualization of Ras proteins in spatially distinct cell surface microdomains. *J Cell Biol* 160: 165-170

Prior IA, Parton RG, Hancock JF (2003b) Observing cell surface signaling domains using electron microscopy. *Sci STKE* 2003: PL9

Pulido R, Stoker AW, Hendriks WJ (2013) PTPs emerge as PIPs: protein tyrosine phosphatases with lipid-phosphatase activities in human disease. *Hum Mol Genet* 22: R66-76

Rehl KM, Selvakumar J, Pitsch RL, Hoang D, Arumugam K, Harshman SW, Gorfe AA, Cho KJ (2023) A new ferrocene derivative blocks K-Ras localization and function by oxidative modification at His95. *Life Sci Alliance* 6

Reiner DJ, Gonzalez-Perez V, Der CJ, Cox AD (2008) Use of Caenorhabditis elegans to evaluate inhibitors of Ras function in vivo. *Methods Enzymol* 439: 425-449

Ripley BD (1977) Modelling spatial patterns. *J R Statist Soc B* 39: 172-192

Robinson FL, Dixon JE (2006) Myotubularin phosphatases: policing 3-phosphoinositides. *Trends Cell Biol* 16: 403-412

Sampaio JL, Gerl MJ, Klose C, Ejsing CS, Beug H, Simons K, Shevchenko A (2011) Membrane lipidome of an epithelial cell line. *Proc Natl Acad Sci U S A* 108: 1903-1907

Schmick M, Vartak N, Papke B, Kovacevic M, Truxius DC, Rossmannek L, Bastiaens PI (2014) KRas localizes to the plasma membrane by spatial cycles of solubilization, trapping and vesicular transport. *Cell* 157: 459-471

Smith MM, Levitan DJ (2004) The Caenorhabditis elegans homolog of the putative prostate cancer susceptibility gene ELAC2, hoe-1, plays a role in germline proliferation. *Dev Biol* 266: 151-160

Sohn M, Ivanova P, Brown HA, Toth DJ, Varnai P, Kim YJ, Balla T (2016) Lenz-Majewski mutations in PTDSS1 affect phosphatidylinositol 4-phosphate metabolism at ER-PM and ER-Golgi junctions. *Proc Natl Acad Sci U S A* 113: 4314-4319

Sohn M, Korzeniowski M, Zewe JP, Wills RC, Hammond GRV, Humpolickova J, Vrzal L, Chalupska D, Veverka V, Fairn GD *et al* (2018) PI(4,5)P2 controls plasma membrane PI4P and PS levels via ORP5/8 recruitment to ER-PM contact sites. *J Cell Biol* 217: 1797-1813

Tan L, Cho KJ, Kattan WE, Garrido CM, Zhou Y, Neupane P, Capon RJ, Hancock JF (2019) Acylpeptide hydrolase is a novel regulator of KRAS plasma membrane localization and function. *J Cell Sci* 132

Tan L, Cho KJ, Neupane P, Capon RJ, Hancock JF (2018) An oxanthroquinone derivative that disrupts RAS plasma membrane localization inhibits cancer cell growth. *J Biol Chem* 293: 13696-13706

Tian T, Harding A, Inder K, Plowman S, Parton RG, Hancock JF (2007) Plasma membrane nanoswitches generate high-fidelity Ras signal transduction. *Nat Cell Biol* 9: 905-914

van der Hoeven D, Cho KJ, Ma X, Chigurupati S, Parton RG, Hancock JF (2013) Fendiline inhibits K-Ras plasma membrane localization and blocks K-Ras signal transmission. *Mol Cell Biol* 33: 237-251

van der Hoeven D, Cho KJ, Zhou Y, Ma X, Chen W, Naji A, Montufar-Solis D, Zuo Y, Kovar SE, Levental KR *et al* (2018) Sphingomyelin Metabolism Is a Regulator of K-Ras Function. *Mol Cell Biol* 38

Varnai P, Balla T (1998) Visualization of phosphoinositides that bind pleckstrin homology domains: calcium- and agonist-induced dynamic changes and relationship to myo-[3H]inositol-labeled phosphoinositide pools. *J Cell Biol* 143: 501-510

Walker DM, Urbe S, Dove SK, Tenza D, Raposo G, Clague MJ (2001) Characterization of MTMR3: an inositol lipid 3-phosphatase with novel substrate specificity. *Curr Biol* 11: 1600-1605

Weinberg F, Schulze E, Fatouros C, Schmidt E, Baumeister R, Brummer T (2014) Expression pattern and first functional characterization of riok-1 in Caenorhabditis elegans. *Gene Expr Patterns* 15: 124-134

Yeung T, Gilbert GE, Shi J, Silvius J, Kapus A, Grinstein S (2008) Membrane phosphatidylserine regulates surface charge and protein localization. *Science* 319: 210-213

Zewe JP, Miller AM, Sangappa S, Wills RC, Goulden BD, Hammond GRV (2020) Probing the subcellular distribution of phosphatidylinositol reveals a surprising lack at the plasma membrane. *J Cell Biol* 219

Zhou Y, Prakash P, Liang H, Cho KJ, Gorfe AA, Hancock JF (2017) Lipid-Sorting Specificity Encoded in K-Ras Membrane Anchor Regulates Signal Output. *Cell* 168: 239-251 e216

Figure 1

A

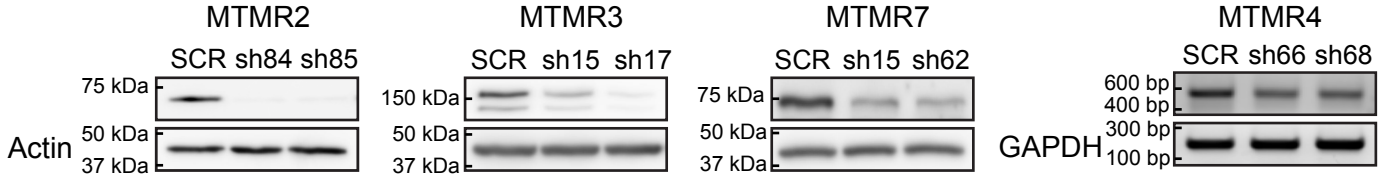


B

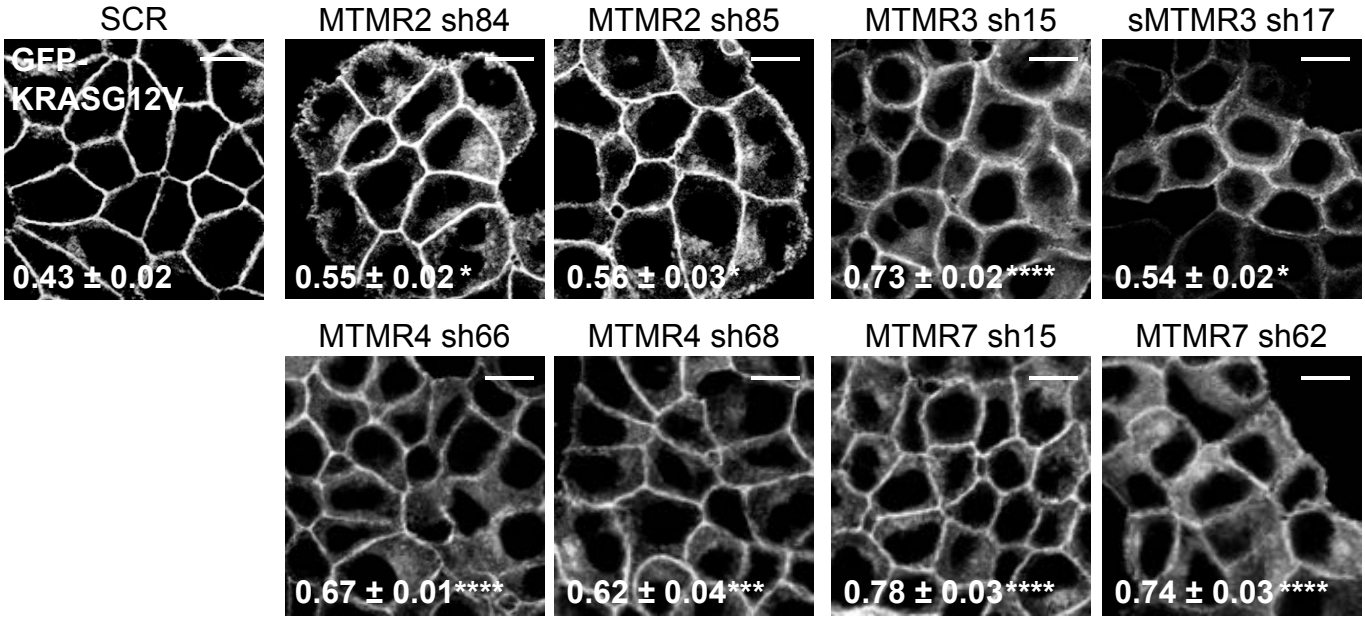


C. GFP-KRASG12V

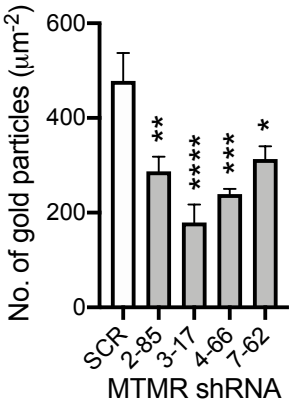


D. GFP-KRASG12V

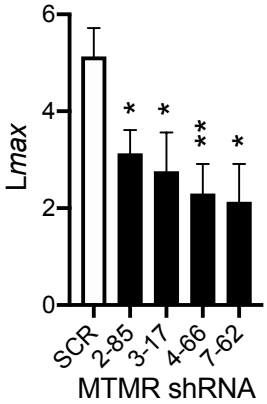

Figure 2

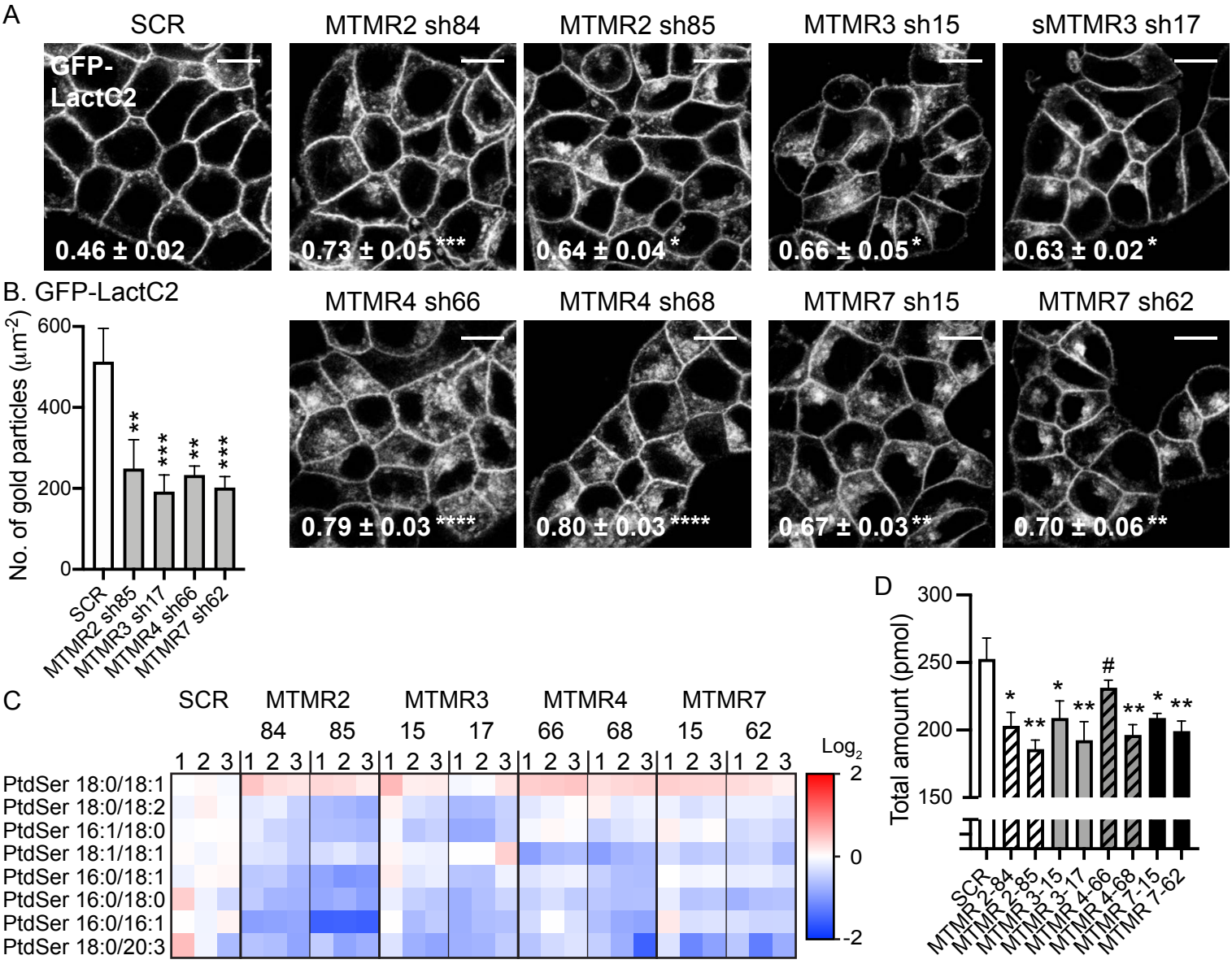
A
SCR
MTMR2 sh84
MTMR2 sh85
MTMR3 sh15
sMTMR3 sh17
GFP-LactC2
0.46 ± 0.02
0.73 ± 0.05 ***
0.64 ± 0.04 *
0.66 ± 0.05 *
0.63 ± 0.02 *
MTMR4 sh66
MTMR4 sh68
MTMR7 sh15
MTMR7 sh62
0.79 ± 0.03 ****
0.80 ± 0.03 ****
0.67 ± 0.03 **
0.70 ± 0.06 **
B. GFP-LactC2
No. of gold particles (μm-2)
600
400
200
0
SCR
MTMR2 sh85
MTMR3 sh17
MTMR4 sh66
MTMR7 sh62
C
SCR
MTMR2
MTMR3
MTMR4
MTMR7
84 85 15 17 66 68 15 62
1 2 3
PtdSer 18:0/18:1
PtdSer 18:0/18:2
PtdSer 16:1/18:0
PtdSer 18:1/18:1
PtdSer 16:0/18:1
PtdSer 16:0/18:0
PtdSer 16:0/16:1
PtdSer 18:0/20:3
Log2
2
0
-2
D
Total amount (pmol)
300
250
200
150
SCR
MTMR 2-84
MTMR 2-85
MTMR 3-15
MTMR 3-17
MTMR 4-66
MTMR 4-68
MTMR 7-15
MTMR 7-62

Figure 3

A

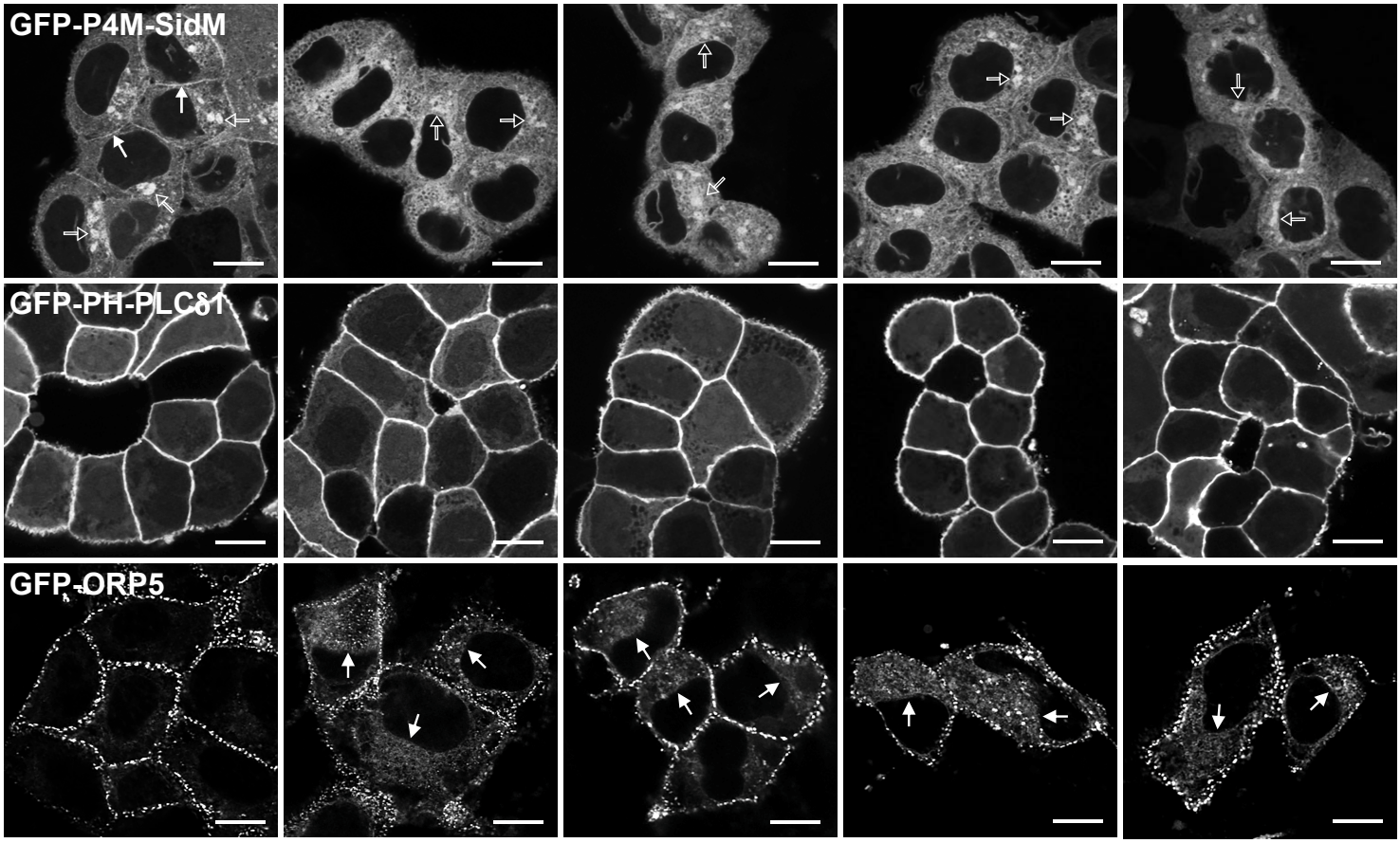


B. GFP-P4M-SidM

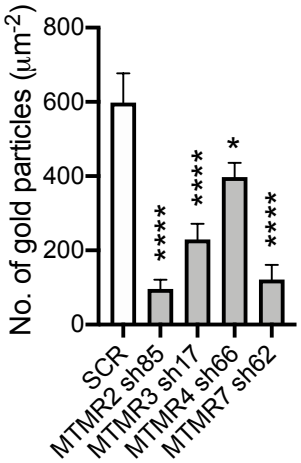


C. GFP-PH-PLCδ1

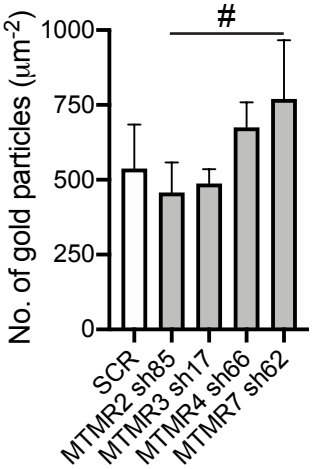

Figure 4

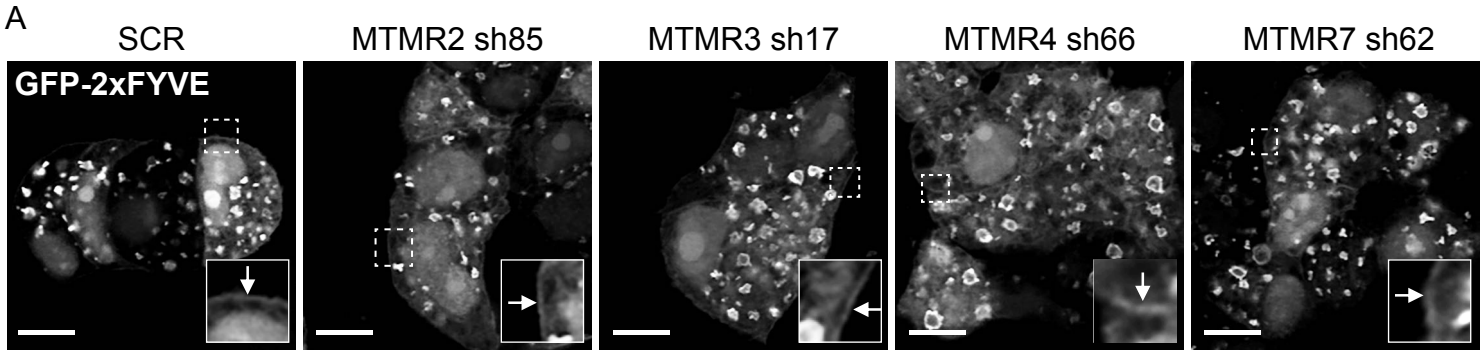
A
SCR
MTMR2 sh85
MTMR3 sh17
MTMR4 sh66
MTMR7 sh62
GFP-2xFYVE

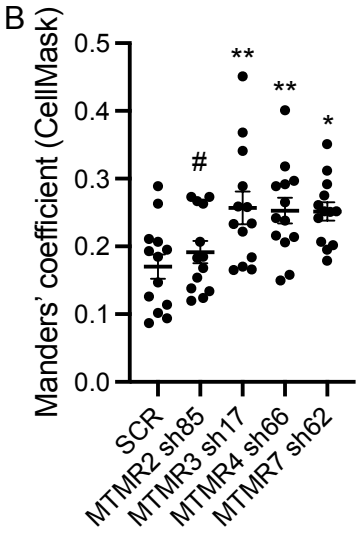
B
Manders' coefficient (CellMask)
0.0
0.1
0.2
0.3
0.4
0.5
#
**
**
*
SCR
MTMR2 sh85
MTMR3 sh17
MTMR4 sh66
MTMR7 sh62

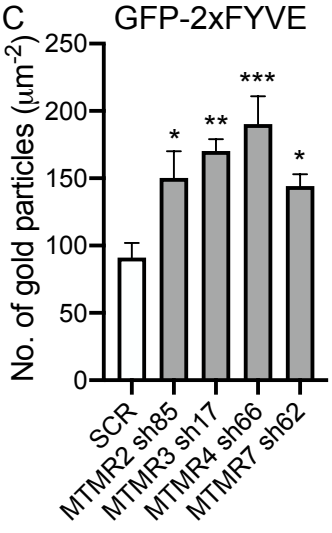
C
GFP-2xFYVE
No. of gold particles (μm-2)
0
50
100
150
200
250
*
**
***
*
SCR
MTMR2 sh85
MTMR3 sh17
MTMR4 sh66
MTMR7 sh62

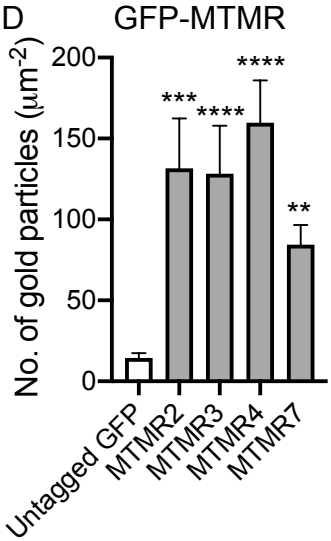
D
GFP-MTMR
No. of gold particles (μm-2)
0
50
100
150
200
***
****
****
**
Untagged GFP
MTMR2
MTMR3
MTMR4
MTMR7

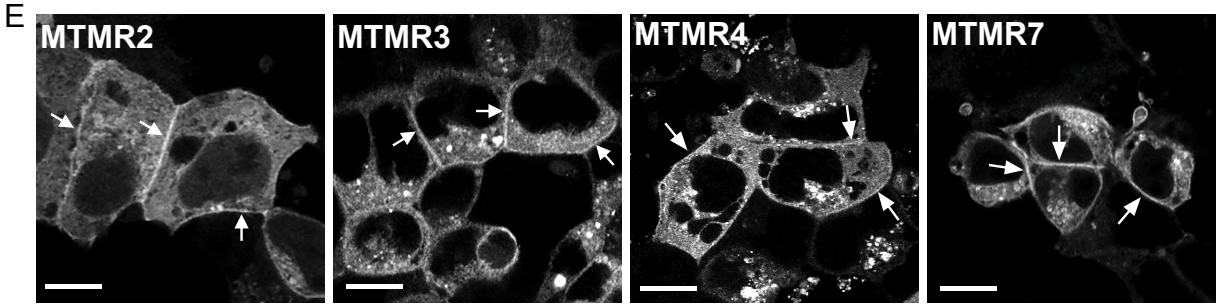
E
MTMR2
MTMR3
MTMR4
MTMR7

Figure 5

A

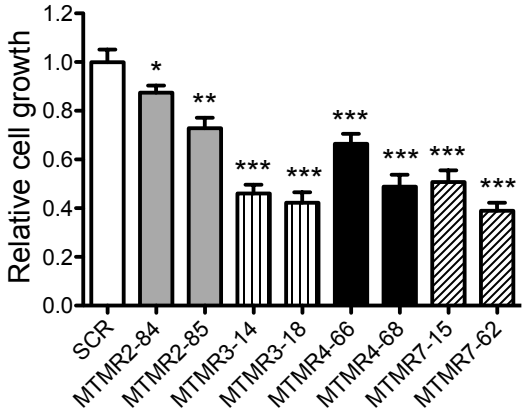
Relative cell growth
1.2
1.0
0.8
0.6
0.4
0.2
0.0
*
**
***
***
***
***
***
***
SCR
MTMR2-84
MTMR2-85
MTMR3-14
MTMR3-18
MTMR4-66
MTMR4-68
MTMR7-15
MTMR7-62

B

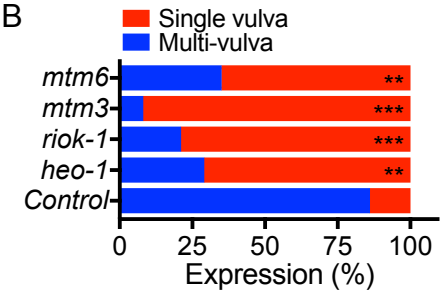
Single vulva
Multi-vulva
mtm6
mtm3
riok-1
heo-1
Control
**
***
***
**
0
25
50
75
100
Expression (%)

Figure 6

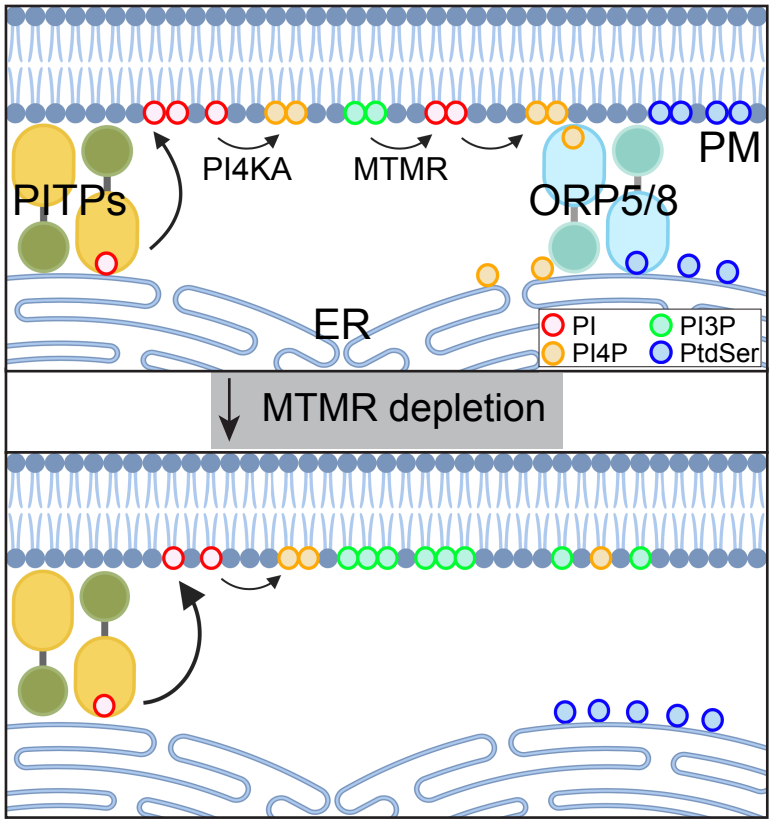
PM
PI4KA
MTMR
PITPs
ORP5/8
ER
PI
PI3P
PI4P
PtdSer
MTMR depletion